

Target-oriented interferometry – Imaging with internal multiples from subsalt VSP data

Ivan Vasconcelos, Roel Snieder*, and Brian Hornby†

*Center for Wave Phenomena, Colorado School of Mines, Golden, CO 80401, USA

†BP America, Inc., Houston, TX 77079, USA

Summary

Seismic interferometry has become a technology of growing interest for imaging from borehole seismic data. We demonstrate that interferometry of internal multiples can be used to image targets above a borehole receiver array. We use an interferometry technique that targets the reconstruction of specific primary reflections from multiply reflected waves. In this *target-oriented* interferometry approach, we rely on shot-domain wavenumber separation to select the directions of waves arriving at a given receiver. We provide a description of this method along with two conceptual applications, and compare it to other approaches to seismic interferometry. Using a numerical walkaway VSP experiment recorded by a subsalt borehole receiver array in the *Sigsbee* salt model, we use the interference of internal multiples to image the salt structure from below. In this numerical example, the interferometric image that targets internal multiples reconstructs the bottom and top salt reflectors above the receiver array, as well as subsalt sediment structure between the array and the salt.

Introduction

Most of exploration seismic imaging is done from surface seismic records. In areas of high structural complexity (e.g., near salt bodies), borehole seismic data may give detailed subsurface information that cannot be obtained from surface seismic data. Hornby et al. (2005) give an example where walkaway VSP data acquired in a subsalt receiver array are used to image sediments below salt that are invisible with surface seismic data.

Current techniques in the field of seismic interferometry (Curtis et al., 2006) open possibilities for innovative uses of borehole seismic data, because seismic interferometry reconstructs waves that propagate between receivers as if one of them acted as a source. Hence, with interferometry, it is possible to “create” pseudo-acquisition geometries that differ from the original physical experiments. Schuster et al. (2004) used the concept of interferometry to migrate free-surface reflections from Reverse VSP data. The Virtual Source method of Bakulin and Calvert (2006) is used to image beneath a complex overburden from borehole sensors placed in a horizontal well with no knowledge of the overburden model parameters. Vasconcelos et al. (2007) used drill-bit noise recordings along with a deconvolution interferometry method to perform the broad-side imaging of the San Andreas fault at Parkfield, CA. In the context of salt flank imaging, Willis et al. (2006) presented a numerical example demonstrating that diving waves can be used for the interferometric imaging of near-vertical salt reflectors.

Although no knowledge of model parameters is necessary for the interferometry of internal multiples, this

method relies on wavefield separation to select waves propagating in specific directions between receivers (Vasconcelos and Snieder, 2007a). For this reason, we refer to this method as *target-oriented* interferometry. Apart from being suitable to image features above the receiver array, target-oriented interferometry can also be tailored to image below the array. In that case, our method is analogous to the Virtual Source applications of Bakulin and Calvert (2006) and Mehta et al. (2007). To perform the interferometry of internal multiples we rely on the two-way representation theorems for perturbed media derived by Vasconcelos and Snieder (2007a).

Target-oriented interferometry

In this section, we describe how to use interferometry to target the illumination of specific regions in the subsurface. We begin by defining the recorded data in the frequency domain as (Vasconcelos and Snieder, 2007a, b)

$$u(\mathbf{r}_A, \mathbf{s}, \omega) = W(\mathbf{s}, \omega) [G_0(\mathbf{r}_A, \mathbf{s}, \omega) + G_S(\mathbf{r}_A, \mathbf{s}, \omega)]; \quad (1)$$

where \mathbf{s} and \mathbf{r}_A are source and receiver locations, respectively, and ω is the angular frequency. The recorded data u is given by the superposition of the unperturbed impulse response G_0 and its perturbation G_S (Vasconcelos and Snieder, 2007a and b). The function $W(\mathbf{s}, \omega)$ describes the excitation at \mathbf{s} . Here, we assume that the medium perturbations that give rise to G_S are localized within the support of a volume \mathbb{P} (Figure 1). For our purposes, it is convenient to assume that both the unperturbed and perturbed portions of the medium (see Figure 1) are heterogeneous. Also, scattering occurs both in the unperturbed and perturbed regimes (e.g., Figure 1a). The objective in our interferometric experiment is to image only G_S : the waves scattered within the perturbation volume \mathbb{P} (Figure 1). These waves are included in the full perturbed response $G(\mathbf{r}_A, \mathbf{r}_B, \omega)$ obtained by interferometry of the full recorded perturbed waves (e.g., Curtis, 2006).

A form of interferometry that targets the extraction of the wavefield perturbation $G_S(\mathbf{r}_A, \mathbf{r}_B, \omega)$, measured at \mathbf{r}_A and excited by a pseudo-source at \mathbf{r}_B is (Vasconcelos and Snieder, 2007a)

$$\int_{\sigma_i} u_S(\mathbf{r}_A, \mathbf{s}) u_0^*(\mathbf{r}_B, \mathbf{s}) d\mathbf{s} \approx \langle |W(\mathbf{s})|^2 \rangle G_S(\mathbf{r}_A, \mathbf{r}_B); \quad (2)$$

where the integration over sources is no longer conducted over the closed surface Σ , but rather over a part of it, denoted by σ_i (e.g., σ_1 or σ_2 in Figure 1).

Interferometric imaging of internal multiples

In order for equation 2 to hold, the sources over σ_1 must sample the stationary points that yield the desired events in $G_S(\mathbf{r}_A, \mathbf{r}_B, \omega)$ (Snieder et al., 2006; Vasconcelos and Snieder, 2007a). Below we describe a method that selects waves in u_0 by wavefield separation.

To perform target-oriented interferometry according to equation 2, we select specific arrivals in u_0 and u_S (Figure 1) with a two-step procedure. First, we choose the segment σ_i based on the relative position of the receivers and the portion of the surface we wish to image (volume \mathbb{P}). For example, the sources over σ_1 excites direct waves that propagate downward and rightward in Figure 1a, that once reflected in the unperturbed medium are recorded as the up-going waves u_0 that are illustrated in the figure. In the case of Figure 1b, the sources over σ_2 are the ones that radiate energy directly down towards the receivers, being thus suitable for reconstructing the desired scattered perturbations from interferometry (see also Bakulin and Calvert, 2006; and Mehta et al., 2007a). In a second step, we separate u_0 and u_S from u according to the direction of the incoming waves at a given receiver. The direction of incoming waves, in the time-domain, can be inferred from the slopes of the arrivals in the recorded shot gathers (i.e., for a fixed source and multiple receivers). In the frequency-wavenumber domain, these slopes translate to the apparent shot-domain wavenumbers, which we refer to as k_s . The choice of which wavenumbers to use at \mathbf{r}_A and \mathbf{r}_B varies from one experiment to another (see Figures 1 and 2).

Figure 2a describes the wavefield separation necessary to target the imaging of scatterers above the receiver array, as in Figure 1a. In this case, keeping the negative shot-domain wavenumbers at \mathbf{r}_B (left-hand side of Figure 2a) defines $u_0(\mathbf{r}_B, \mathbf{s}, \omega)$ (equation 2), which contains mostly up-going incoming waves. This ensures that the pseudo-source at \mathbf{r}_B (see equation 2) radiates mostly up-going energy. For the receivers that record the interferometric data, represented by \mathbf{r}_A , the choice of incoming wave direction depends on the relative positioning between a given receiver and the pseudo-source at \mathbf{r}_B . If the receiver is above the pseudo-source (top cartoon on right-hand side of Figure 2a), waves with $k_s < 0$ give $u_S(\mathbf{r}_A, \mathbf{s}, \omega)$ (see equation 2). For \mathbf{r}_A below \mathbf{r}_B , we use waves with $k_s > 0$ to extract $u_S(\mathbf{r}_A, \mathbf{s}, \omega)$.

To image below the receiver array, as in Figure 1b, wavefield separation can be done according to Figure 2b. For the pseudo-source at \mathbf{r}_B , we select the down-going incoming waves $u_0(\mathbf{r}_B, \mathbf{s}, \omega)$ excited by the sources over σ_2 (Figure 1b) by preserving arrivals with $k_s > 0$ (left-hand cartoon in Figure 2b). Keeping waves with $k_s < 0$ at the recording receivers in the interferometry experiment yields $u_S(\mathbf{r}_A, \mathbf{s}, \omega)$ (right-hand cartoon in Figure 2b). This criterium for the extraction of $u_S(\mathbf{r}_A, \mathbf{s}, \omega)$ from $u(\mathbf{r}_A, \mathbf{s}, \omega)$ is the same for receivers that are either above or below the pseudo-source. After wavefield separation as in Figure 2b, using $u_S(\mathbf{r}_A, \mathbf{s}, \omega)$ and $u_0(\mathbf{r}_B, \mathbf{s}, \omega)$ for different \mathbf{r}_A positions results in a pseudo-shot gather that radiates energy down toward the perturbation volume \mathbb{P} (Figure 1b). As mentioned above, the case of Figure 1b is also the objective of the Virtual Source

method (Bakulin and Calvert, 2006; Mehta et al., 2007a).

Interferometry by deconvolution (Vasconcelos and Snieder, 2007) is an option for reconstructing an interferometric impulse response when estimates of the source power spectra are not available. When estimates of the power spectra of the source function are available, these can be used to extract the impulse response from interferometry (Wapenaar and Fokkema, 2006; Mehta et al., 2007a). In particular, deconvolution interferometry can be more effective than its correlation-based counterpart in reconstructing impulsive pseudo-sources when the input excitation consists of a complicated, unknown waveform (Vasconcelos and Snieder, 2007b). This can be the case when using internal multiples to do interferometry. Here, apart from using correlation interferometry, we rely on a deconvolution interferometry method (Vasconcelos and Snieder, 2007b) to create impulsive images from our data examples.

Subsalt imaging from VSP data

We present an example that consists of a subsalt walkaway (WAW) VSP numerical experiment using the *Sigsbee* velocity model. The purpose of this numerical example is to use the subsalt WAW VSP data to image the Sigsbee salt canopy from below by using the interference of internal multiples, analogous to the example in Figure 1. The experiment simulates the recording of shots placed 500 ft deep, at 100 evenly-spaced receivers in a deviated borehole (red lines in Figures 3 and 4). The first receiver is placed at $x = 48000$ ft and at a depth of 16000 ft; while the lateral and depth coordinates of the last receiver are 52950 ft and 20950 ft, respectively. The shots start at $x = 10000$ ft with a shot interval of 125 ft. The source waveform consists of a Ricker wavelet with 12 Hz peak frequency. In our experiments, we consider shots placed from $x = 10000$ ft to $x = 53500$ ft (this corresponds to the surface σ_1 in Figure 1a).

Interferometric images using the full recorded data (with no wavefield separation) are shown in Figure 3. The imaging in these examples is done by wavefield extrapolation in a slant coordinate system that conforms with the receiver array. Wavefield extrapolation is done by the Split-step Fourier Phase-shift-plus-interpolation method (Biondi, 2006). Figure 3a is generated using cross-correlation interferometry while Figure 3b is obtained from deconvolution interferometry after source summation (Vasconcelos and Snieder, 2007b). The source function is suppressed by deconvolution interferometry (Figure 3b; Vasconcelos and Snieder, 2007b). The images in Figure 3 show an accurate reconstruction of the salt canopy, especially towards the right-hand side of the model where the salt flanks are dipping. Above the receiver array, the imaged salt is characterized by reflectors that are weak compared to the dipping salt flanks. The images of the sediments between the salt the receiver array are distorted and do not reproduce the horizontal bedding of the model (Figure 3).

After applying the target-oriented interferometry method based on wavefield separation illustrated by Figure 2a, we obtain the images in Figure 4. Note that although the original source and receiver geometry is the same for the images in Figures 3 and 4 is the

Interferometric imaging of internal multiples

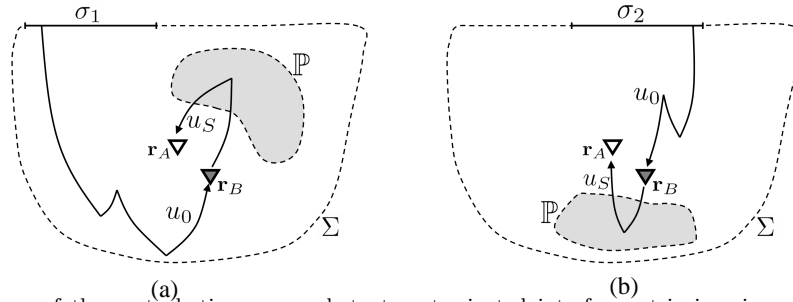


Fig. 1: Illustrations of the perturbation approach to target-oriented interferometric imaging. A large volume is bounded by the surface Σ , that contains medium perturbations that are restricted to the volume \mathbb{P} (indicated by the grey-shaded areas). Closed surfaces are denoted by the dashed lines. In both panels, u_0 are unperturbed wavefields, while u_S are wavefield perturbations due to scattering within the volume \mathbb{P} . The solid lines illustrate stationary wave-paths. Two receivers, located at \mathbf{r}_A and \mathbf{r}_B , are represented by the triangles. The grey triangle denotes the receiver that acts as a pseudo-source in the interferometric experiments. When the target is imaging medium perturbations above the receivers, as in panel (a), we rely on waves excited by sources over the surface σ_1 (solid black line). In panel (b), interferometry targets the reconstruction of up-going scattered waves from below the receivers. In this case, we consider only waves generated by sources on the surface σ_2 .

same, the portion of the model illuminated by these two sets of images is substantially different. As discussed in the previous Section, the pseudo-sources reconstructed by target-oriented interferometry are designed to radiate energy upward (Figures 1a and 2a). Hence, the images in Figure 4 illuminate the model predominantly in the area above the receiver array. These images show bright reflectors at the bottom and top salt above the array, which appear as dim reflectors in the images in Figure 4. Figure 4b shows that the target-oriented interferometric images recover the structure of the subsalt sediments which are not seen in Figure 3. The reflector that corresponds to the dipping top salt (right-hand side of images in Figure 3) is not present in the images in Figure 4. This reflector is absent in the target oriented interferometric images because it is imaged in Figure 3 from reflections reconstructed from diving waves that arrive at the receiver array with positive shot-domain wavenumbers. Since the wavefield separation builds the filter u_0 from $k_s < 0$, reflectors from such diving waves are not present in Figure 4.

Discussion and Conclusions

We present an interferometry technique based on wavefield separation in the shot-domain that targets the reconstruction of specific arrivals in the interferometric shot gathers. In particular, we promote that this target-oriented interferometry technique can be used to reconstruct single-reflected waves from internal multiples. The application of the technique consists in manipulating the recorded data to separate unperturbed waves at the receiver that acts as a pseudo-source, and wavefield perturbations at the receivers that record the interferometric experiment. We separate these wavefields according to the directions of the waves incoming at a given receiver; i.e., according to the shot-domain wavenumber.

Using the *Sigsbee* salt model, we illustrate how interferometric illumination can be controlled using wavefield separation along with the appropriate choice of sources to be included. The numerical experiment consists of a large-offset walkaway VSP recorded at a deviated 100-receiver array placed below the salt. Seismic interferometry with no wavefield separation

yields an image of the salt body which is well defined in the dipping salt flanks to the right-hand side of the array. These reflectors are mainly sampled by diving waves, analogously to the numerical experiment by Willis et al. (2006). The images obtained from target-oriented interferometry recover the reflectors at the top and base of salt located immediately above the receiver array. These images also recover a portion the subsalt sediment structure that cannot be retrieved by the interferometry of the full recorded wavefields. In the *Sigsbee* example, the target-oriented interferometry procedure reconstructs down-going single-scattered waves from up-going internal multiples recorded in the original experiment.

The interferometric experiments we present in this paper are not necessarily restricted to active-shot VSP experiments and P-wave imaging. The same experiments could be conceived in the context of passive seismic measurements (e.g., Draganov et al., 2006) or in the interferometric imaging of drill-bit noise records (Vasconcelos and Snieder, 2007c). Draganov et al. (2006) present a methodology to recover elastic pseudo-shot records using seismic interferometry. Likewise, target-oriented interferometry can be potentially designed to recover multicomponent subsalt pseudo-shot records. Such records, along with surface seismic data, can help in better understanding the local physical structure in subsalt environments. This understanding may come in the form of more realistic models of the subsalt velocity field that incorporate anisotropy as well as lateral parameter variations. As in the *Sigsbee* numerical example, long receiver arrays can help in obtaining interferometric images with a wide image aperture: each receiver added to an array contributes with a source and a receiver to the interferometry experiment.

Acknowledgements

This research was financed by the NSF (grant EAS-0609595) and by the sponsors of the Consortium for Seismic Inverse Methods for Complex Structures at the Center for Wave Phenomena.

Interferometric imaging of internal multiples

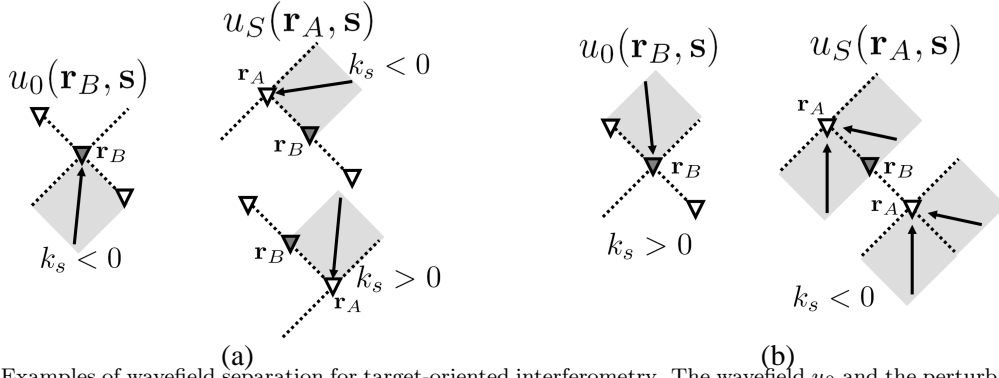


Fig. 2: Examples of wavefield separation for target-oriented interferometry. The wavefield u_0 and the perturbation u_S are extracted from the recorded perturbed wavefield u by wavefield separation. Wavefield separation is implemented by wavenumber filtering (e.g., by $f - k$ filtering) in the shot domain. Receivers are represented by triangles. The receiver that acts as a pseudo-source (located at \mathbf{r}_B) is indicated by the grey triangles. The arrows indicate the direction of waves arriving at the receivers. The directions parallel and perpendicular to the receiver line define a coordinate frame indicated by the dashed lines. In this coordinate frame, k_s is the shot-domain wavenumber of a given recorded wave. Panel (a) illustrates the separation of wavefields necessary for target-oriented interferometric imaging in the context of Figure 1a. The wavefield separation in panel (b) is designed for the imaging experiment in Figure 1b.

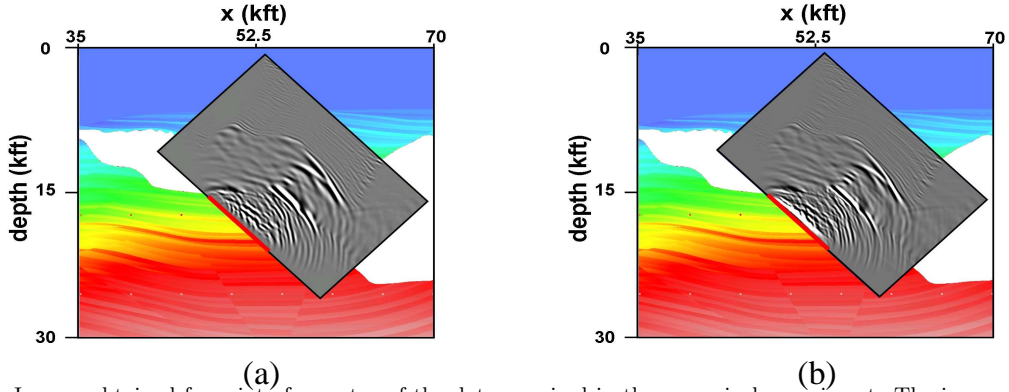


Fig. 3: Images obtained from interferometry of the data acquired in the numerical experiment. The images, in grey scale, are superposed on the *Sigsbee* velocity model. The images are based on cross-correlation interferometry (panel a), and on deconvolution interferometry (panel b). We used the full wavefield recorded at the receivers to reconstruct the interferometric shot gathers from which these images are obtained.

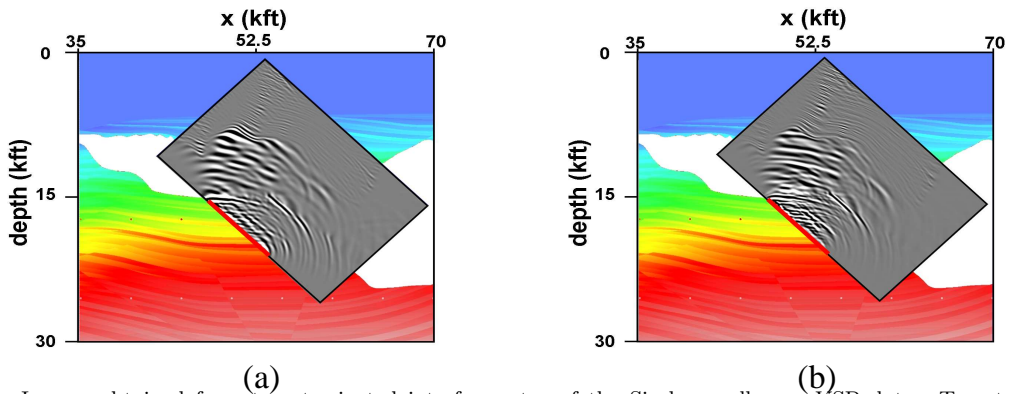


Fig. 4: Images obtained from target-oriented interferometry of the *Sigsbee* walkaway VSP data. Target-oriented interferometry is implemented with the wavefield separation approach described in Figure 2a. As in Figure 3, the image in (a) is obtained from cross-correlation interferometry and the image in (b) from deconvolution interferometry. The reflectors in these images come from single-reflections reconstructed by interferometry mostly from internal multiples. This numerical experiment is analogous to that shown in Figure 1a.